nature climate change

Article

https://doi.org/10.1038/s41558-022-01562-8

Temperature effect on erosion-induced disturbances to soil organic carbon cycling

Received: 30 January 2022

Accepted: 21 November 2022

Published online: 30 January 2023

Check for updates

Zhengang Wang[1,2,8], Yizhe Zhang[2,8], Gerard Govers[3], Guoping Tang[2], Timothy A. Quine[4], Jianxiu Qiu[2], Ana Navas[5], Haiyan Fang[6], Qian Tan[1] & Kristof Van Oost[7]

Erosion exerts control on soil organic carbon (SOC) and both erosion and SOC are affected by climate. To what extent temperature controls the coupling between these erosion–C interactions remains unclear. Using ^{137}Cs and SOC inventories from catchments spanning different climates, we find that increasing decomposition rates with temperature result in the efficient replacement of SOC laterally lost by erosion in eroding areas but lower preservation of deposited SOC in depositional areas. When combined at the landscape level, the erosion-induced C sink strength per unit lateral SOC flux increases with temperature from 0.19 g C (g C)$^{-1}$ at 0 °C to 0.24 g C (g C)$^{-1}$ at 25 °C. We estimated that the global C sink of 0.050 Pg C yr^{-1} induced by water erosion on croplands increases by 7% because of climate change. Our results reveal a negative feedback loop between climate change and erosion-induced disturbance to SOC cycling.

Soils store more carbon than the atmosphere and vegetation combined, thereby offering a large potential to mitigate climate change via C sequestration[1,2]; at the same time, soils also pose a threat as global warming and agricultural expansion might release parts of this large stock[3–7]. Soil organic C (SOC) storage is controlled by the balance between C inputs and decomposition, both of which are mediated by climate[8,9]. SOC stocks and turnover times are known to covary with climate globally[10,11] but the relationship is complex: the sensitivity of SOC cycling to temperature change is higher in cold regions than in warm regions[11] and different ecosystems have different degrees of sensitivity and coping mechanisms adapting to climate warming[4,5,12,13]. It is therefore not surprising that the response of SOC to climate change is among the largest uncertainties under future climate change projections[3,8,14,15].

Erosion causes a large flux of SOC across the land-to-ocean aquatic continuum (LOAC)[16–18], especially when natural land cover is converted to croplands[19,20]. These lateral SOC fluxes exert substantial impacts on C cycling processes along the LOAC and result in notable amounts of C exchange between land and atmosphere[21,22]. Previous studies focusing on the aquatic system showed that these disturbances of erosion to the C cycling are also modulated by temperature. For instance, organic C in the riverine water and sediments was found to decompose more rapidly with increasing temperature resulting in higher CO_2 evasion from rivers in warm regions[23,24]. Similarly, the decomposition rate of buried organic C in lakes was found to increase with temperature[25,26].

As is the case of mobilized sediments entering aquatic environments, temperature is expected to affect C dynamics in eroding uplands as well, where most C mobilized by erosion is redeposited[27–29]. In eroding areas, the reduced SOC stocks (due to SOC erosion) will decrease soil heterotrophic respiration, which, in combination with continued photosynthesis, results in a net uptake of atmospheric C by the soil. This C uptake replaces parts of the SOC lost laterally by erosion, a process that is referred to as 'dynamic replacement'[30–33].

[1]Guangdong Provincial Key Laboratory of Water Quality Improvement and Ecological Restoration for Watersheds, Institute of Environmental and Ecological Engineering, Guangdong University of Technology, Guangzhou, China. [2]Key Laboratory of Urbanization and Geo-simulation of Guangdong Province, School of Geography and Planning, Sun Yat-sen University, Guangzhou, China. [3]Division of Geography, Department of Earth and Environmental Sciences, KU Leuven, Leuven, Belgium. [4]Geography, College of Life and Environmental Sciences, University of Exeter, Exeter, UK. [5]Soil and Water Department, Estación Experimental de Aula Dei (EEAD-CSIC), Zaragoza, Spain. [6]Key Laboratory of Water Cycle and Related Land Surface Processes, Institute of Geographic Sciences and Natural Resources Research, Chinese Academy of Sciences, Beijing, China. [7]Georges Lemaître Center for Earth and Climate Research (TECLIM), Earth and Life Institute, Université Catholique de Louvain, Louvain-la-Neuve, Belgium. [8]These authors contributed equally: Zhengang Wang, Yizhe Zhang. e-mail: wangzhg33@mail.sysu.edu.cn

In depositional areas, the lateral influx of SOC leads to a disequilibrium between the SOC stock and local vegetation inputs. The buried sediments will therefore lose more SOC by microbial decomposition than they gain SOC through vegetation inputs and SOC stored in deposited sediments declines after burial[34–36]. The ratio between the preserved organic C in buried sediments and the originally deposited SOC is termed C burial efficiency (CBE)[37,38]. Thus, erosion brings fresh soil minerals from deeper horizons to the surface where they are mixed with and adsorb some of the C derived from vegetation[39]. During the geomorphic cascade of erosion, transport and deposition, a fraction of the fixed C is decomposed, while the remaining is preserved in burial sites often characterized by low decomposition rates, resulting in a net sink of atmospheric C at the scale of eroding landscapes[21,40]. While both C inputs and SOC decomposition depend on temperature, the effects of temperature on the replacement of SOC lost from the eroding areas and the preservation of buried SOC in the depositional areas have hitherto not been explored. Therefore, the relationship between temperature and the efficacy of the C sink resulting from the operation erosion and subsequent sediment burial can, at present, not be fully assessed and it remains uncertain how this C sink will respond to climate change.

Here, we investigated the temperature effects on erosion–C coupling via three lines of evidence. First, we compiled a dataset from the literature of SOC and ^{137}Cs inventories of agricultural soils in Asia, Europe and North America spanning a wide range of climatic conditions (Extended Data Fig. 1 and Supplementary Table 1). In total, 1,562 profiles from 20 catchments including stable and erosional soils at upland hillslopes as well as colluvial soils at footslopes were examined. The artificial fallout radioisotope ^{137}Cs was used as a tracer to determine lateral soil and SOC redistribution rates (erosion and deposition rates). The direction and magnitude of net exchanges of C with the atmosphere were derived from field observations of SOC stocks and soil redistribution rates (SRRs) at stable, eroding and depositional sites. The effect of temperature on erosion–C coupling was assessed by confronting the SOC cycling characteristics with the mean annual temperature of each catchment. Second, we used a model that combines a SOC cycling module with soil redistribution processes to simulate SOC dynamics at the hillslope scale in eroding landscapes as a function of temperature (Supplementary Methods Section 6). The model was run in a series of scenarios with different C input and decomposition conditions to explore how temperature affects the erosion–C coupling via changing the C input and decomposition rates. Third, by combining global estimates of SOC stocks and of agricultural soil erosion rates[21], we estimated the global lateral SOC fluxes on croplands in relation to surface erosion (Supplementary Methods Section 5). The same erosion–C integrated model was applied at the global scale to investigate how the erosion–C coupling varies with temperature.

Erosion–C coupling in upland catchments

As observed in previous studies[41], SOC stocks decreased with temperature (Fig. 1a), indicating a more rapid increase of SOC decomposition rate than SOC input with temperature. Within each catchment, SOC stocks were positively correlated with SRRs with eroding areas depleted of SOC and depositional areas enriched in SOC (Extended Data Fig. 2). To avoid the influence of SOC stock differences on the comparison between catchments, we normalized the SOC stock by dividing them by the average SOC stock of the stable sites within each catchment. The slope of the regression line between the SRRs (derived from ^{137}Cs inventories) and the normalized SOC stock represents the sensitivity of the (normalized) SOC stock to the variation of SRRs for each catchment. As shown in Fig. 1b, the slope of the regression lines decreased with increasing temperature, indicating that SOC stocks are more sensitive to soil redistribution in cold regions than in warm regions.

Numerical simulations of SOC dynamics at the hillslope scale (Supplementary Methods Section 6) demonstrated that SOC stocks changed linearly with SOC inputs (Extended Data Fig. 3a) and that the spatial variation of normalized SOC stocks was independent of variations of SOC inputs (Extended Data Fig. 3b). In contrast, an increase of SOC decomposition rates not only decreased total SOC stocks (Extended Data Fig. 4a) but also decreased the spatial variation of SOC stocks (Extended Data Fig. 4b). When both SOC input and decomposition rates were allowed to vary with temperature, the spatial variability of SOC stocks would decrease with temperature (Fig. 1b and Extended Data Fig. 5b). This is because in eroding areas the C replacement ratio of the laterally exported SOC increased with temperature, while in depositional areas the burial efficiency of deposited SOC decreased with temperature (Extended Data Fig. 5c).

In line with model predictions, field observations showed that the average C replacement ratio of the eroding profiles increased with temperature from ~65.0% at 0 °C to ~87.5% at 25 °C (Fig. 1c). This indicates that the C sink effect in the eroding area increases with temperature. A linear regression between soil redistribution (independent variable) and the burial efficiency of deposited SOC (dependent variable) showed that the slope of regression lines decreased with increasing temperature (Fig. 1d). This indicates that CBE decreased more rapidly with depositional rates in warm regions than in cold regions. Thus, the difference between areas subjected to soil redistribution and reference areas becomes smaller with increasing temperature, as eroded SOC is more rapidly replaced and deposited SOC is less efficiently preserved in warmer environments. Consequently, reduced SOC variability with soil redistribution at the landscape scale is observed in warm regions (Fig. 1b).

The overall and integrated influence of temperature on erosion-induced C exchange at the scale of upland catchment is determined by the balance between the increase of C replacement with temperature in eroding areas (more C replaced in warm regions) and the decrease of CBE with temperature in depositional areas (more C lost in warm regions). Model simulations suggest that the combination of these two counteracting processes will result in an increase of the efficiency of the C sink per unit lateral SOC flux (the ratio of erosion-induced land–atmosphere C exchanges to lateral SOC fluxes due to erosion) with increasing temperature (Extended Data Fig. 5d). The empirical data also suggest an increase of the C sink strength per unit lateral SOC flux but this trend is not statistically significant (Fig. 1e). Thus, in colder climates where C turnover is slower, the dominant effect of soil erosion is to cause a physical redistribution of SOC, thereby having less impact on the C exchange between soil and atmosphere. In ecosystems characterized by faster C decomposition rates, higher C replacement ratios of the laterally lost SOC result in a more efficient pathway to sequester atmospheric CO_2 from the atmosphere at eroding sites. At depositional sites, the soil–atmosphere C exchange is also enhanced but in the opposite direction, leading to higher losses of C from the soil to the atmosphere as temperature increases. Carbon sequestration in eroding areas increases more rapidly with temperature than C loss in depositional areas, so that the overall erosion sink becomes larger with increasing temperature.

Erosion–C coupling at the global scale

The temperature effects on erosion–C interactions at the global scale were explored using available spatial datasets in a spatially explicit approach (Supplementary Methods Section 5). The net primary productivity (NPP) was regarded as an estimate of the vegetation C inputs to soils based on the assumption that the vegetation biomass is at steady state[11]. We acknowledge that some regions are subjected to disturbances such as land use change and fires and are at a transition stage. Nevertheless, since the remote sensing-derived NPP (resolution 30 arcsec) and Harmonized World Soil Database derived from SOC profiles (resolution 30 arcsec) represent the average condition of the raster grid, they can be regarded as an approximation of the equilibrium condition of the area. At the global scale, both NPP and SOC decomposition rates (estimated by dividing NPP by SOC stocks) increased

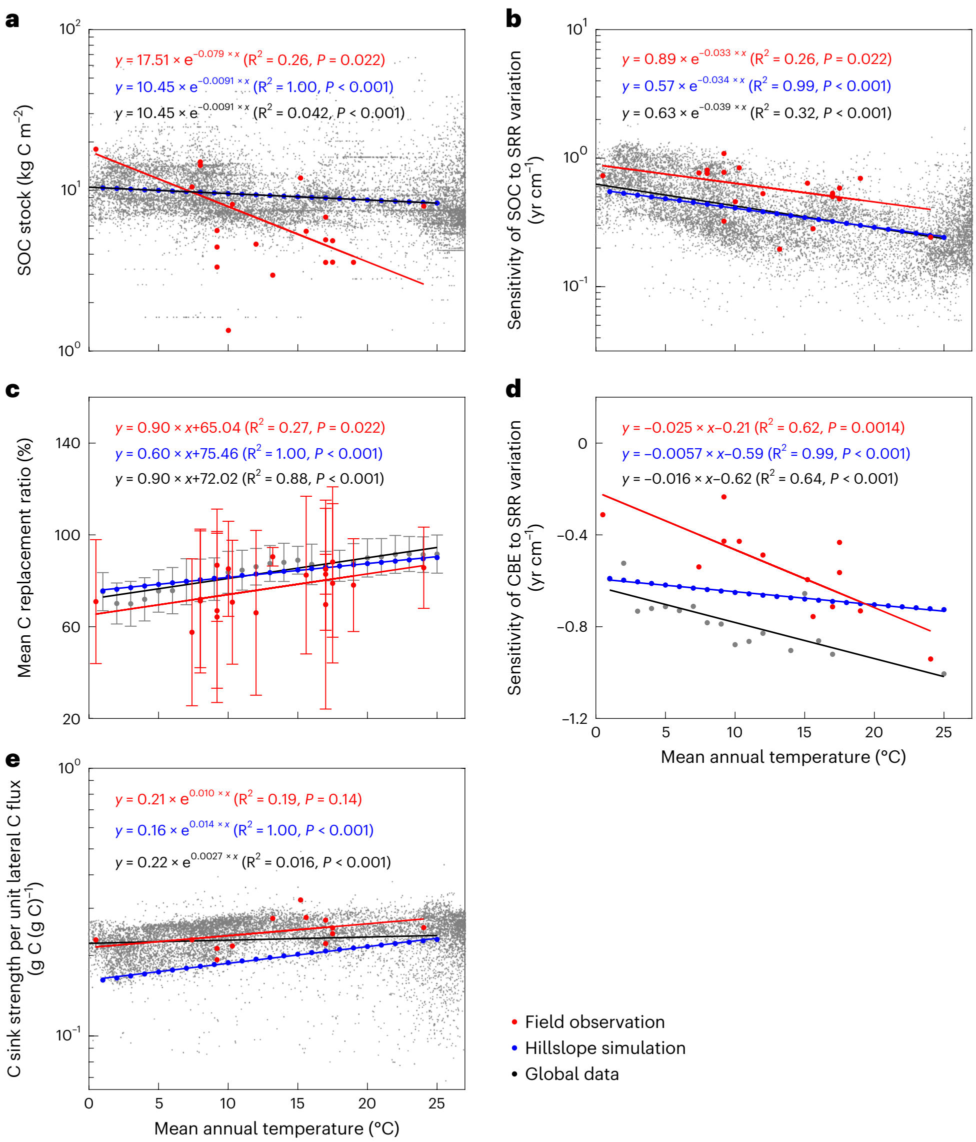

Fig. 1 | Variation of SOC cycling metrics on eroding croplands with temperature. **a**, Variation of SOC stocks (top 1 m) with temperature. **b**, Variation of the slope of linear regression lines between the SRR (independent variable) and the normalized SOC stock (dependent variable) with temperature. **c**, Variation of the average replacement ratio of SOC laterally lost by erosion with temperature. **d**, Variation of the slope of linear regression lines between the SRR (independent variable) and the CBE (dependent variable) with temperature. **e**, Variation of the C sink strength per unit lateral SOC flux with temperature. The red points denote the observations from the cropland sites, the blue points denote the results of hillslope scale model simulations and the grey points denote the results of global model simulations. The lines are the regression curves of the points of the same colour. Texts denote the regression equations of points of the same colour. Error bars denote the standard deviation. SRR in **b** and **d** denotes soil redistribution rate and CBE in **d** denotes C burial efficiency. One-sided *F*-test was used in the regression analysis. The sample numbers of field observations of each cropland site are displayed in Supplementary Table 1.

with temperature, while SOC stocks decreased with temperature (Fig. 2). To assess the temperature sensitivity of SOC cycling processes, we used the concept of Q_{10} values, that is the factor by which a given SOC cycling metric varies for a 10 °C increase in temperature[42]. We obtained a globally averaged Q_{10} value of 1.43 for the SOC decomposition rate, which is in line with earlier estimates[11,43]. Due to this positive relationship between SOC decomposition rates and temperature, the C replacement ratio of laterally lost SOC by erosion was found to increase with temperature while the CBE of deposited SOC decreased with temperature (Fig. 1). In line with the field data interpretation and hillslope scale model simulations, the magnitude of the erosion-induced C sink per unit of lateral SOC flux was positively correlated with temperature increasing from ~0.19 g C (g C)$^{-1}$ at 0 °C to ~0.24 g C (g C)$^{-1}$ at 25 °C at the global scale (Fig. 2d).

To assess the C sink strength per unit cropland area, it is also necessary to consider the absolute magnitude of the lateral SOC fluxes. As reported in previous studies[21,44], we estimated global soil and C erosion to be 17.89 and 0.26 Pg yr^{-1}, respectively. We obtained a global C sink of 0.050 Pg C yr^{-1} induced by water erosion on croplands (Fig. 3). This estimate is lower than the one obtained by ref. [21] because the latter included both water and tillage erosion on croplands as well as agricultural erosion on pasture and rangelands. The water erosion rate of croplands was found to be positively related to the mean annual precipitation at the global scale[21] (Extended Data Fig. 6a). Since mean annual precipitation was positively related to mean annual temperature (Extended Data Fig. 6b), the water erosion rate on croplands was also positively correlated with mean annual temperature globally (Extended Data Fig. 6c). This explains why, despite a negative correlation between

https://doi.org/10.1038/s41558-022-01562-8

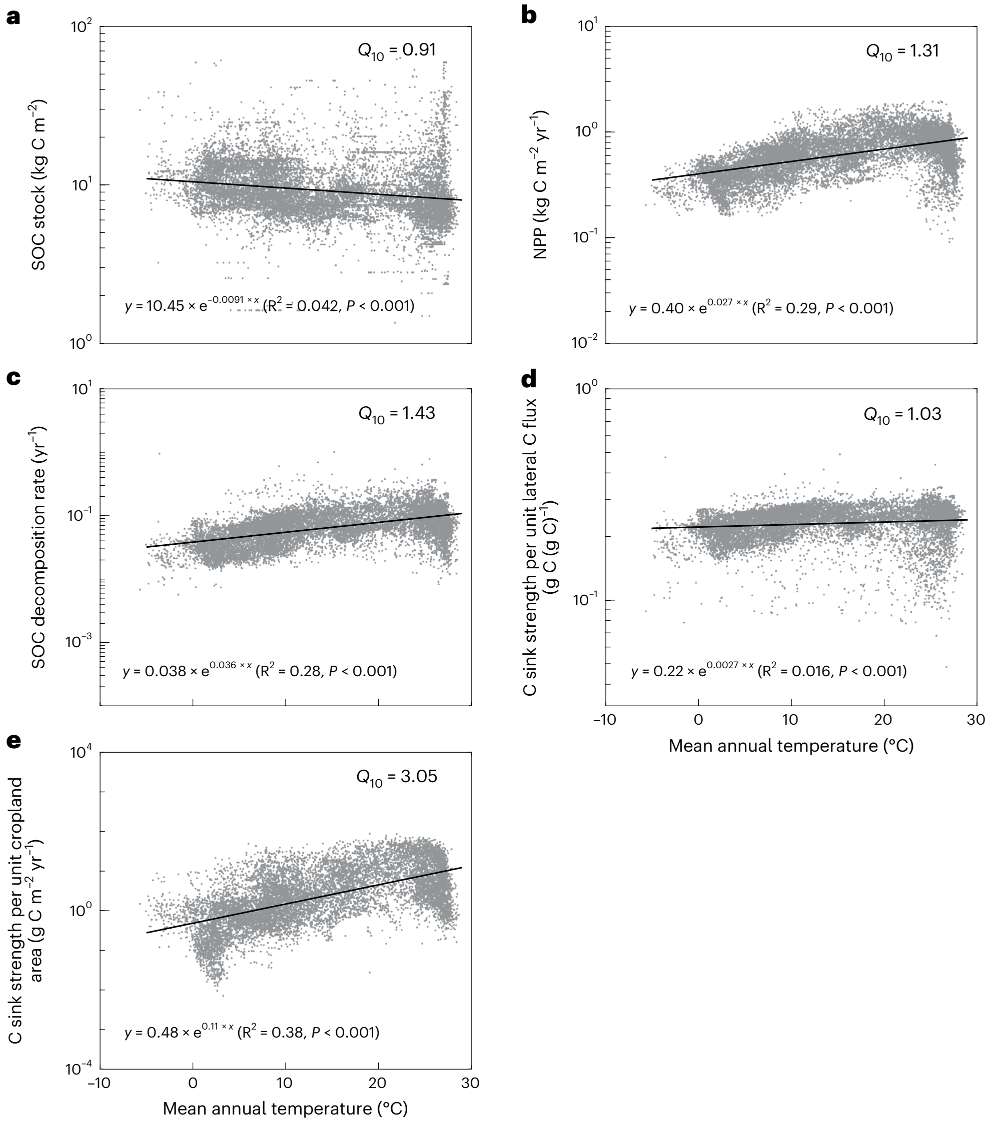

Fig. 2 | Temperature effects on SOC cycling metrics on eroding croplands at the global scale. a, Variation of SOC stocks (top 1 m) with temperature. **b**, Variation of NPP with temperature. **c**, Variation of SOC decomposition rates with temperature. **d**, Variation of the C sink strength per unit lateral C flux. **e**, Variation of the C sink strength per unit cropland area with temperature. Lines are the regression curves of corresponding SOC cycling metrics and texts denote the regression equations. One-sided *F*-test was used in the regression analysis.

SOC stocks and temperature, the C erosion rate of croplands and the erosion-induced C sink per unit cropland area were positively correlated with temperature (Fig. 2e and Extended Data Fig. 6d). C erosion rates show an exponential increase with temperature[21], which explains why the Q_{10} value for the C sink per unit cropland area (3.05) is much higher than the Q_{10} value for the C sink per unit lateral SOC flux (1.03).

The relationships between various SOC cycling metrics and temperature derived from the three independent lines of research were consistent with each other (Fig. 1) but the strength of the relationships varied due to differences in methods, scales and datasets. The SOC stock variability caused by soil redistribution derived from model simulations is lower than that obtained from field data (Fig. 1b), which is probably related to the fact that the model did not take into account the relationships between soil redistribution and SOC inputs to soils with lower C inputs in eroding areas due to the negative effect of erosion on crop productivity[45,46]. An assessment based on ^{137}Cs and C stock inventory data showed that the spatial variability of crop productivity due to soil redistribution accounted for 35.5 ± 25.1% of the spatial variability of SOC stocks, confirming that the erosion–C input relation is indeed important (Supplementary Methods Section 12). In addition, C burial efficiencies were closely related to the SRR (Extended Data Fig. 5c) and tests showed that the difference in the SRRs among the datasets used in different methods accounted for the main source of differences between model simulations at the hillslope and global scales (Supplementary Figs. 8 and 9).

Erosion–C coupling under climate change

We applied a space-for-time approach to assess the potential variation of temperature effects on SOC cycling in croplands due to future climate change (Supplementary Methods Section 10). The SOC cycling metrics (for example, SOC stock, NPP and erosion) under future climate projections generated by eight global climate models in four scenarios (Supplementary Tables 2 and 3) were estimated using the exponential relationships between these metrics and climatic factors (temperature and precipitation). As predicted in previous studies[3,47], we estimated a SOC stock decline of 4.1 ± 1.6% in croplands in 2100 (Fig. 4).

https://doi.org/10.1038/s41558-022-01562-8

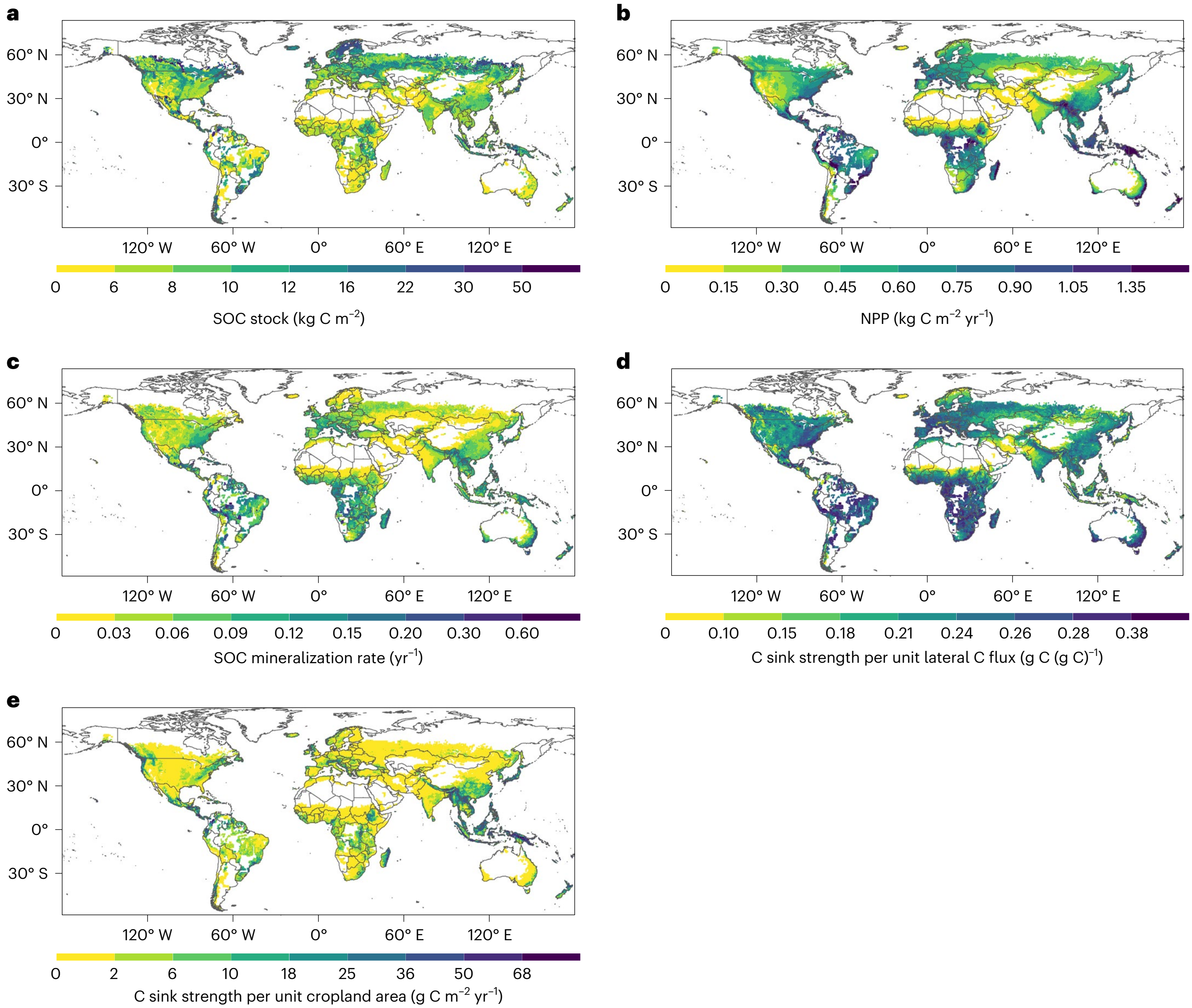

Fig. 3 | Spatial variation of SOC cycling metrics on eroding croplands. a, SOC stocks (top 1 m). **b**, NPP. **c**, SOC decomposition rates. **d**, The C sink strength per unit lateral C flux. **e**, The C sink strength per unit cropland area.

Increasing precipitation under future climate projections could result in an increase of 17.9 ± 8.6% in water erosion on croplands, which is lower than a previous estimate that suggested an increase of well over 30% (ref. [48]). The integrated effects of SOC stock and erosion variation cause the lateral SOC flux by water erosion on croplands to increase by 6.3 ± 7.2%. The C sink efficiency per unit lateral SOC flux would increase by 1.1 ± 1.4% due to global warming and the total C sink by water erosion on croplands was predicted to increase by 7.4 ± 6.2%.

Numerical simulations of SOC cycling at the global scale under different soil moisture conditions demonstrated that the SOC decomposition rate peaked at an intermediate soil moisture of 0.29 $m^3\ m^{-3}$ under present climatic conditions. This rate was 50% higher than the SOC decomposition rates under either dry (0.16 $m^3\ m^{-3}$) or wet (0.40 $m^3\ m^{-3}$) conditions (Supplementary Fig. 4 and Extended Data Fig. 7b). While important to recognize, this soil moisture effect on SOC decomposition was significantly smaller than the effect of temperature, where the SOC decomposition rate at 25 °C was ~2.5 times that at 0 °C (Fig. 2c). Because of the positive correlation between the C sink per unit lateral SOC flux and SOC decomposition rates, the variation of the C sink per unit lateral SOC flux with soil moisture was similar to the variation of the SOC decomposition rate with soil moisture (Supplementary Fig. 5 and Extended Data Fig. 7c). The C sink strength per unit cropland area is largely controlled by the SOC erosion rate. Since lateral SOC fluxes were higher in areas where soil moisture is higher as both the SOC flux and soil moisture are positively related to mean annual precipitation (Supplementary Fig. 3 and Extended Data Fig. 7a), the C sink strength per unit cropland area also increased with increasing soil moisture (Supplementary Fig. 6 and Extended Data Fig. 7d). Soil moisture effects under projected future climates were similar to those for the present climate (Extended Data Fig. 7), with the limited differences being due to differences between present and future lateral soil fluxes rather than variations in soil moisture per se.

In summary, our analysis, based on multiple lines of evidence, shows strong support for the proposition that temperature is an important control on the magnitude of erosion-induced disturbances to the SOC cycling in croplands. We found that the C replacement ratio of

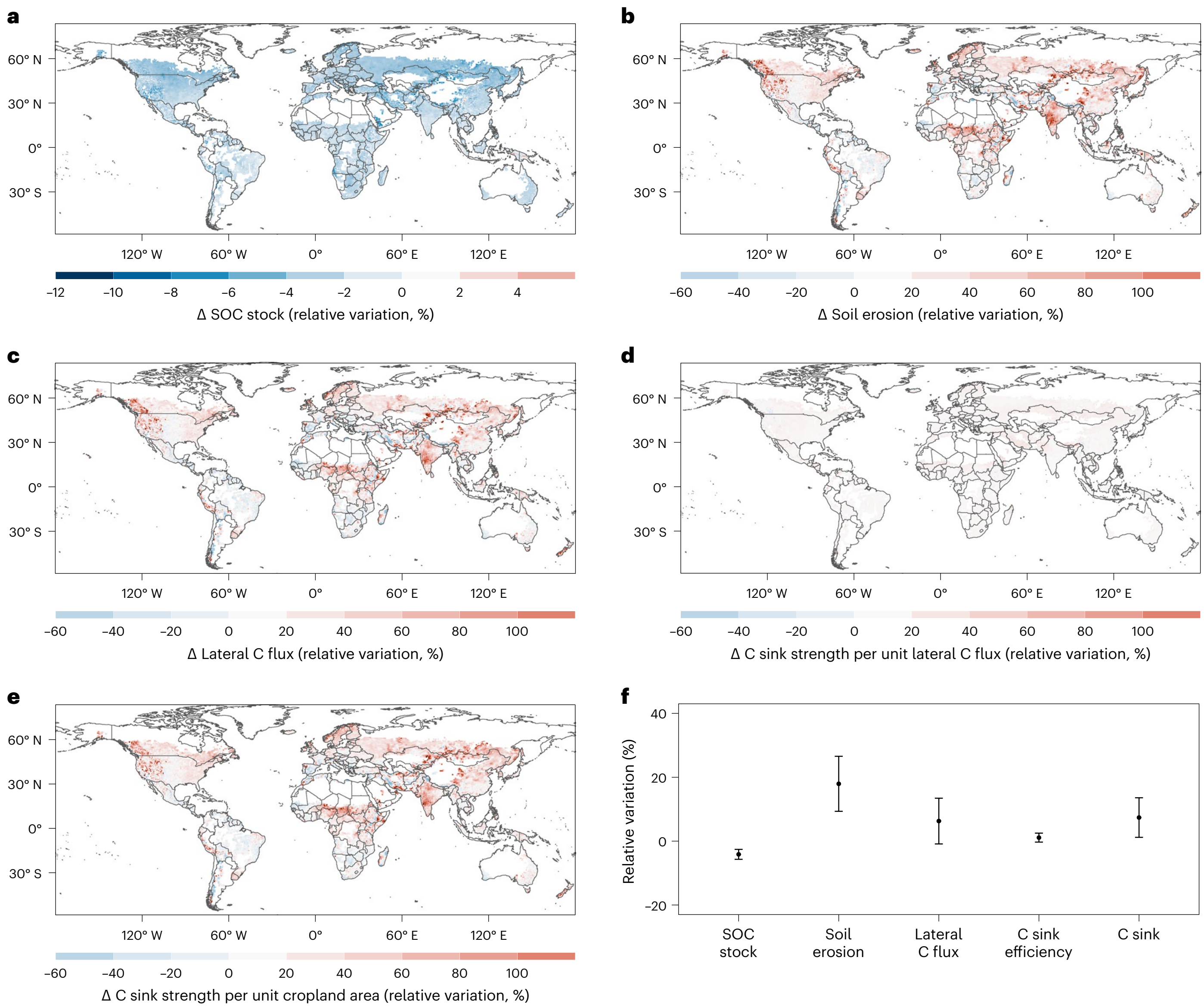

Fig. 4 | Response of SOC cycling in eroding croplands to climate change. a–f, Relative variation of SOC stocks (**a**), soil erosion (**b**), the lateral SOC flux due to erosion (**c**), the C sink strength per unit lateral SOC flux (**d**), the C sink strength per unit cropland area (**e**) caused by erosion in 2100 and the statistics of them (**f**). Error bars in **f** denote the standard deviation.

SOC that is laterally lost by erosion increases with temperature, while the CBE of deposited SOC decreases with temperature. This results in a larger landscape-scale spatial variation of SOC stocks due to erosion in cold regions than in warm regions. Model simulations revealed that increasing C decomposition rates with temperature are the main factor controlling the spatial heterogeneity of SOC cycling in eroding landscapes, while increasing C inputs with temperature exert the same impacts in both eroding and depositional areas. Our results also show that the erosion-induced C sink per unit lateral SOC flux increases with temperature. The positive relation between sink strength and temperature is further enhanced by the fact that C erosion rates are also positively related to temperature. Together these mechanisms cause a significant increase of the C sink per unit cropland area with temperature. Previous studies had revealed that lateral SOC fluxes due to erosion exert an important impact on global C cycling[16,21,22] and this impact is mediated by the erosion intensity[35]. Our results improve our understanding of the complexity of geomorphology–biogeochemistry interactions by adding the effects of temperature. Variations in temperature not only affect C erosion directly but also change the in situ SOC cycling responses to the erosion-induced lateral SOC fluxes. The variability of erosion–C coupling with temperature presented in our analysis implies that a more detailed assessment of the spatial variability of erosion-induced SOC cycling disturbances is required to fully understand the feedback loop between SOC cycling and climate changes (Fig. 4). In the context of exacerbated erosion by climatic extremes and future global warming[49–51], soil redistribution would play a more important role in global C cycling. Substantial C emission from soils is expected in the future global warming[3–5,52]; however, this net emission would cease when SOC stocks reach a new equilibrium. In contrast, the C uptake caused by erosion and subsequent burial functions as long as erosion occurs. Our results show that increasing temperature also enhances the erosion-induced C sink that could potentially offset a small fraction of the C emission from soils due to global warming. This effect is analogous to the widely recognized negative feedback loop between silicate weathering and climate change[53,54]. Nevertheless, in the immediate future, efforts to replace lost SOC in eroded landscapes through erosion control may yield net C-sequestration benefits in the pursuit of global net-zero objectives.

Online content

Any methods, additional references, Nature Portfolio reporting summaries, source data, extended data, supplementary information, acknowledgements, peer review information; details of author contributions and competing interests; and statements of data and code availability are available at https://doi.org/10.1038/s41558-022-01562-8.

References

1. Lal, R. Soil carbon sequestration impacts on global climate change and food security. *Science* **304**, 1623–1627 (2004).
2. Amundson, R. et al. Soil and human security in the 21st century. *Science* **348**, 1261071 (2015).
3. Crowther, T. W. et al. Quantifying global soil carbon losses in response to warming. *Nature* **540**, 104–108 (2016).
4. Nottingham, A. T., Meir, P., Velasquez, E. & Turner, B. L. Soil carbon loss by experimental warming in a tropical forest. *Nature* **584**, 234–237 (2020).
5. Xue, K. et al. Tundra soil carbon is vulnerable to rapid microbial decomposition under climate warming. *Nat. Clim. Change* **6**, 595–600 (2016).
6. Houghton, R. A. & Nassikas, A. A. Global and regional fluxes of carbon from land use and land cover change 1850–2015. *Glob. Biogeochem. Cycles* **31**, 456–472 (2017).
7. Hicks Pries, C. E., Castanha, C., Porras, R. C. & Torn, M. S. The whole-soil carbon flux in response to warming. *Science* **355**, 1420–1423 (2017).
8. Davidson, E. A. & Janssens, I. A. Temperature sensitivity of soil carbon decomposition and feedbacks to climate change. *Nature* **440**, 165–173 (2006).
9. Mahecha, M. D. et al. Global convergence in the temperature sensitivity of respiration at ecosystem level. *Science* **329**, 838–840 (2010).
10. Carvalhais, N. et al. Global covariation of carbon turnover times with climate in terrestrial ecosystems. *Nature* **514**, 213–217 (2014).
11. Koven, C. D., Hugelius, G., Lawrence, D. M. & Wieder, W. R. Higher climatological temperature sensitivity of soil carbon in cold than warm climates. *Nat. Clim. Change* **7**, 817–822 (2017).
12. Sistla, S. A. et al. Long-term warming restructures Arctic tundra without changing net soil carbon storage. *Nature* **497**, 615–618 (2013).
13. Dorrepaal, E. et al. Carbon respiration from subsurface peat accelerated by climate warming in the subarctic. *Nature* **460**, 616–619 (2009).
14. Karhu, K. et al. Temperature sensitivity of soil respiration rates enhanced by microbial community response. *Nature* **513**, 81–84 (2014).
15. Knorr, W., Prentice, I. C., House, J. I. & Holland, E. A. Long-term sensitivity of soil carbon turnover to warming. *Nature* **433**, 298–301 (2005).
16. Galy, V., Peucker-Ehrenbrink, B. & Eglinton, T. Global carbon export from the terrestrial biosphere controlled by erosion. *Nature* **521**, 204–207 (2015).
17. Stallard, R. F. Terrestrial sedimentation and the carbon cycle: coupling weathering and erosion to carbon burial. *Glob. Biogeochem. Cycles* **12**, 231–257 (1998).
18. Regnier, P. et al. Anthropogenic perturbation of the carbon fluxes from land to ocean. *Nat. Geosci.* **6**, 597–607 (2013).
19. Montgomery, D. R. Soil erosion and agricultural sustainability. *Proc. Natl Acad. Sci. USA* **104**, 13268–13272 (2007).
20. Cerdan, O. et al. Rates and spatial variations of soil erosion in Europe: a study based on erosion plot data. *Geomorphology* **122**, 167–177 (2010).
21. Van Oost, K. et al. The impact of agricultural soil erosion on the global carbon cycle. *Science* **318**, 626–629 (2007).
22. Chappell, A., Baldock, J. & Sanderman, J. The global significance of omitting soil erosion from soil organic carbon cycling schemes. *Nat. Clim. Change* **6**, 187–191 (2016).
23. Raymond, P. A. et al. Global carbon dioxide emissions from inland waters. *Nature* **503**, 355–359 (2013).
24. Lauerwald, R., Laruelle, G. G., Hartmann, J., Ciais, P. & Regnier, P. A. G. Spatial patterns in CO_2 evasion from the global river network. *Glob. Biogeochem. Cycles* **29**, 534–554 (2015).
25. Gudasz, C. et al. Temperature-controlled organic carbon mineralization in lake sediments. *Nature* **466**, 478–481 (2010).
26. Marotta, H. et al. Greenhouse gas production in low-latitude lake sediments responds strongly to warming. *Nat. Clim. Change* **4**, 467–470 (2014).
27. Rommens, T. et al. Soil erosion and sediment deposition in the Belgian loess belt during the Holocene: establishing a sediment budget for a small agricultural catchment. *Holocene* **15**, 1032–1043 (2005).
28. Phillips, J. D. Fluvial sediment budgets in the North Carolina Piedmont. *Geomorphology* **4**, 231–241 (1991).
29. Trimble, S. W. & Crosson, P. U.S. Soil erosion rates—myth and reality. *Science* **289**, 248–250 (2000).
30. Harden, J. W. et al. Dynamic replacement and loss of soil carbon on eroding cropland. *Glob. Biogeochem. Cycles* **13**, 885–901 (1999).
31. Billings, S. A., Buddemeier, R. W., Richter, D. D., Van Oost, K. & Bohling, G. A simple method for estimating the influence of eroding soil profiles on atmospheric CO_2. *Glob. Biogeochem. Cycles* **24**, GB2001 (2010).
32. Berhe, A. A., Harden, J. W., Torn, M. S. & Harte, J. Linking soil organic matter dynamics and erosion-induced terrestrial carbon sequestration at different landform positions. *J. Geophys. Res. Biogeosci.* **113**, G04039 (2008).
33. Nadeu, E., Berhe, A. A., de Vente, J. & Boix-Fayos, C. Erosion, deposition and replacement of soil organic carbon in Mediterranean catchments: a geomorphological, isotopic and land use change approach. *Biogeosciences* **9**, 1099–1111 (2012).
34. Wang, Z. et al. The fate of buried organic carbon in colluvial soils: a long-term perspective. *Biogeosciences* **11**, 873–883 (2014).
35. Wang, Z., Van Oost, K. & Govers, G. Predicting the long-term fate of buried organic carbon in colluvial soils. *Glob. Biogeochem. Cycles* **29**, 65–79 (2015).
36. VandenBygaart, A. J., Kroetsch, D., Gregorich, E. G. & Lobb, D. Soil C erosion and burial in cropland. *Glob. Change Biol.* **18**, 1441–1452 (2012).
37. Burdige, D. J. Burial of terrestrial organic matter in marine sediments: a re-assessment. *Glob. Biogeochem. Cycles* **19**, GB4011 (2005).
38. Sobek, S. et al. Organic carbon burial efficiency in lake sediments controlled by oxygen exposure time and sediment source. *Limnol. Oceanogr.* **54**, 2243–2254 (2009).
39. Doetterl, S. et al. Erosion, deposition and soil carbon: a review of process-level controls, experimental tools and models to address C cycling in dynamic landscapes. *Earth Sci. Rev.* **154**, 102–122 (2016).
40. Wang, Z. et al. Human-induced erosion has offset one-third of carbon emissions from land cover change. *Nat. Clim. Change* **7**, 345–349 (2017).
41. Jobbágy, E. G. & Jackson, R. B. The vertical distribution of soil organic carbon and its relation to climate and vegetation. *Ecol. Appl.* **10**, 423–436 (2000).
42. Meyer, N., Welp, G. & Amelung, W. The temperature sensitivity (Q10) of soil respiration: controlling factors and spatial prediction at regional scale based on environmental soil classes. *Glob. Biogeochem. Cycles* **32**, 306–323 (2018).

43. Zhou, T., Shi, P., Hui, D. & Luo, Y. Global pattern of temperature sensitivity of soil heterotrophic respiration (Q10) and its implications for carbon–climate feedback. *J. Geophys. Res. Biogeosci.* **114**, G02016 (2009).
44. Doetterl, S., Van Oost, K. & Six, J. Towards constraining the magnitude of global agricultural sediment and soil organic carbon fluxes. *Earth Surf. Process. Landf.* **37**, 642–655 (2012).
45. Kosmas, C. et al. The effects of tillage displaced soil on soil properties and wheat biomass. *Soil Tillage Res.* **58**, 31–44 (2001).
46. Dercon, G. et al. Spatial variability in crop response under contour hedgerow systems in the Andes region of Ecuador. *Soil Tillage Res.* **86**, 15–26 (2006).
47. Lugato, E., Lavallee, J. M., Haddix, M. L., Panagos, P. & Cotrufo, M. F. Different climate sensitivity of particulate and mineral-associated soil organic matter. *Nat. Geosci.* **14**, 95–300 (2021).
48. Borrelli, P. et al. Land use and climate change impacts on global soil erosion by water (2015–2070). *Proc. Natl Acad. Sci. USA* **117**, 21994–22001 (2020).
49. Min, S.-K., Zhang, X., Zwiers, F. W. & Hegerl, G. C. Human contribution to more-intense precipitation extremes. *Nature* **470**, 378–381 (2011).
50. Li, Z. & Fang, H. Impacts of climate change on water erosion: a review. *Earth Sci. Rev.* **163**, 94–117 (2016).
51. Sutton, R. T. & Hawkins, E. ESD ideas: global climate response scenarios for IPCC assessments. *Earth Syst. Dynam.* **11**, 751–754 (2020).
52. Walker, T. W. N. et al. Microbial temperature sensitivity and biomass change explain soil carbon loss with warming. *Nat. Clim. Change* **8**, 885–889 (2018).
53. Berner, R. A., Lasaga, A. C. & Garrels, R. M. The carbonate–silicate geochemical cycle and its effect on atmospheric carbon dioxide over the past 100 million years. *Am. J. Sci.* **283**, 641–683 (1983).
54. Gaillardet, J., Dupré, B., Louvat, P. & Allègre, C. J. Global silicate weathering and CO_2 consumption rates deduced from the chemistry of large rivers. *Chem. Geol.* **159**, 3–30 (1999).

Publisher's note Springer Nature remains neutral with regard to jurisdictional claims in published maps and institutional affiliations.

Springer Nature or its licensor (e.g. a society or other partner) holds exclusive rights to this article under a publishing agreement with the author(s) or other rightsholder(s); author self-archiving of the accepted manuscript version of this article is solely governed by the terms of such publishing agreement and applicable law.

© The Author(s), under exclusive licence to Springer Nature Limited 2023

Methods

Soil profile database analysis

Soil profiles with SOC and ^{137}Cs inventories from 20 agricultural catchments in Asia, Europe and North America were compiled from the literature (Extended Data Fig. 1). In total, 1,562 profiles including stable and erosional soils at upland hillslopes as well as colluvial soils at footslopes were examined. The SRRs at the decadal scale were derived from ^{137}Cs inventories using a conversion model that takes into account factors such as plough layer depth and sampling year[21]. The effects of soil redistribution on the SOC cycling were assessed via the following set of metrics.

First, the C replacement ratio (CRR, %), which is the ratio of the replaced C by the new C supplemented from photosynthesis to the continuous C loss from the top soil layers by erosion, was calculated:

$$\mathrm{CRR} = \frac{\Delta \mathrm{VC_e}}{C_\mathrm{e}} \times 100\% \quad (1)$$

Where ΔVC_e (kg C m^{-2}) is the cumulative erosion-induced C uptake from the atmosphere for the eroding profiles and C_e (kg C m^{-2}) is the cumulative lost SOC by erosion.

Second, the CBE (%), which is the ratio between the preserved organic C in buried sediments and the originally deposited SOC, was calculated:

$$\mathrm{CBE} = \frac{C_1}{C_0} \times 100\% \quad (2)$$

where C_1 (kg C m^{-2}) is the preserved organic C in buried sediments and C_0 (kg C m^{-2}) is the originally deposited SOC.

Third, to assess the sensitivity of SOC stocks to soil erosion rate variations, a linear regression between normalized SOC stocks and SRRs was performed for each agricultural catchment:

$$\mathrm{SOC_n} - 1 = a \times R \quad (3)$$

Where SOC_n is the normalized SOC stock being divided by the SOC stock of reference positions not subjected to erosion or deposition, R (cm yr^{-1}) is the SRR with negative values indicating erosion and positive values indicating deposition and a (yr cm^{-1}) is a coefficient. Steep regression lines indicate high sensitivities of SOC stocks to soil redistribution variations.

Fourth, to assess the sensitivity of CBE to deposition rate variations, a linear regression between CBE and ^{137}Cs-derived soil deposition rate was performed for each site:

$$\mathrm{CBE} - 100\% = b \times D \quad (4)$$

Where CBE (%) is the CBE of the bulk deposited SOC, D (cm yr^{-1}) is the deposition rate and b (yr cm^{-1}) is a coefficient.

A simple box model was used to estimate erosion-induced C exchange for agricultural profiles[40,55,56], which is based on the concept that the SOC stock variation for a soil profile during a period is the result of cumulative soil–atmosphere C exchanges and the cumulative lateral SOC fluxes by erosion. The effects of temperature on the erosion–C coupling were assessed by confronting various metrics with the mean annual temperature of each catchment (Supplementary Methods).

Model simulations at the hillslope scale

Since temperature mediates both C inputs and decomposition, we used a model that combines SOC cycling with soil redistribution processes to disassemble the effects of C input and decomposition on erosion–C coupling. The SOC cycling processes were represented using a one-pool C model, which included SOC fluxes such as C input and decomposition. SOC decomposition was assumed to follow first-order kinetics. Soil profiles in the model were represented as discrete layers and SOC dynamics were simulated in each layer independently. Carbon inputs to soils and SOC decomposition rates were set to decrease exponentially with soil depth[57,58]. The model tracks the C depth profile evolution caused by the soil removal in eroding areas and the soil accumulation in depositional areas. The SOC content of each layer was updated by mixing the soils from different layers of the previous time step. Details of the model are provided in the Supplementary Methods. The model was run in a series of scenarios with different C input and decomposition conditions at an 'ideal' hillslope with a standard soil redistribution pattern to test how these temperature-mediated factors affect SOC cycling in eroding landscapes.

Model estimations at the global scale

The variability of erosion-induced C exchanges between atmosphere and land under different climatic conditions at the global scale was estimated using existing datasets. Global estimates of agricultural erosion[21] were combined with the SOC stock to estimate the lateral SOC flux by erosion. The model tracked the mobilization and burial of SOC from sources to sinks and the in situ SOC dynamics were simulated using the above one-pool SOC cycling model under the condition of soil redistribution. NPP was used as an approximate of SOC inputs. Similarly, the sensitivity of SOC stock to soil redistribution variations, C replacement ratio of laterally lost SOC by erosion in eroding areas, CBE of deposited SOC in depositional areas and erosion-induced C exchanges between land and atmosphere were assessed. Details of the estimation are provided in the Supplementary Methods.

Model predictions under climate change projections

In this study, we used future climate projections generated by eight global climate models (Supplementary Table 2) in four socioeconomic and representative concentration pathway scenarios (Supplementary Table 3). A space-for-time approach was applied to assess the variation of the effects of erosion on SOC cycling in eroding croplands. Using the exponential relationship between C cycling metrics (for example, SOC stock, NPP and erosion) and climatic factors (temperature and precipitation), we calculated the C cycling metrics under future climatic conditions based on the C cycling metrics of present day and the variation of climatic factors. With the derived SOC stocks, NPP and erosion rate above, the effects of erosion on the SOC cycling on croplands in various climate scenarios were assessed as described in Supplementary Methods.

Data availability

The SOC stock of the top 1 m generated by the Harmonized World Soil Database is available at https://www.fao.org/soils-portal/data-hub/soil-maps-and-databases/harmonized-world-soil-database-v12/en/. The SOC stock of the top 1 m generated by the Northern Circumpolar Soil Carbon Database is available at https://bolin.su.se/data/ncscd/tiff.php. The MODIS NPP dataset is available at http://files.ntsg.umt.edu/data/NTSG_Products/MOD17/GeoTIFF/MOD17A3/. The land use data generated by the History database of the Global Environment (HYDE) is available at https://dataportaal.pbl.nl/downloads/HYDE/. The mean annual temperature provided by the Climatic Research Unit is available at https://www.uea.ac.uk/web/groups-and-centres/climatic-research-unit/data. The mean annual precipitation provided by the Global Precipitation Climatology Centre is available at https://opendata.dwd.de/climate_environment/GPCC/html/fulldata-monthly_v2018_doi_download.html. The MODIS potential evapotranspiration (PET) data are available at http://files.ntsg.umt.edu/data/NTSG_Products/MOD16/MOD16A3.105_MERRAGMAO/. The mean annual temperature and mean annual precipitation as well as the surface soil moisture (0–10 cm) of historical simulations and future projections generated by global climate models of coupled model intercomparison project (CMIP6) are available at https://esgf-node.llnl.gov/projects/cmip6/.

The basemap data used to create figures were downloaded at http://naturalearthdata.com/downloads/. The ^{137}Cs inventory and SOC stock data are available from the corresponding author on request. Source data are provided with this paper.

Code availability

The codes of C–erosion coupling model programmed in MATLAB are available at https://doi.org/10.5281/zenodo.7224539 (ref. [59]).

References

55. Quine, T. A. & Van Oost, K. Quantifying carbon sequestration as a result of soil erosion and deposition: retrospective assessment using caesium-137 and carbon inventories. *Glob. Change Biol.* **13**, 2610–2625 (2007).
56. Van Oost, K. et al. Legacy of human-induced C erosion and burial on soil–atmosphere C exchange. *Proc. Natl Acad. Sci. USA* **109**, 19492–19497 (2012).
57. Van Oost, K. et al. Landscape-scale modeling of carbon cycling under the impact of soil redistribution: the role of tillage erosion. *Glob. Biogeochem. Cycles* **19**, GB4014 (2005).
58. Gerwitz, A. & Page, E. R. An empirical mathematical model to describe plant root systems. *J. Appl. Ecol.* **11**, 773–781 (1974).
59. Wang, Z. Erosion-C model. *Zenodo* https://doi.org/10.5281/zenodo.7224539 (2022).

Acknowledgements

Z.W., G.T. and J.Q. are funded by the Natural Science Foundation of China (grant no. 42171025 and 41971031). A.N. is funded by the MCIN/AEI/10.13039/501100011033/ (grant no. PID2019-104857RB-I00 and PID2019-103946RJ-100).

Author contributions

Z.W. and Y.Z. conceived the research, performed the analysis and co-wrote the paper. G.G., G.T., T.A.Q., J.Q., A.N., H.F., Q.T. and K.V.O. assisted in the interpretation of the results and commented on the manuscript.

Competing interests

The authors declare no competing interests.

Additional information

Extended data is available for this paper at https://doi.org/10.1038/s41558-022-01562-8.

Supplementary information The online version contains supplementary material available at https://doi.org/10.1038/s41558-022-01562-8.

Correspondence and requests for materials should be addressed to Zhengang Wang.

Peer review information *Nature Climate Change* thanks Asmeret Berhe, Julian Campo, Amaury Frankl, Priyanka Singh and the other, anonymous, reviewer(s) for their contribution to the peer review of this work.

Reprints and permissions information is available at www.nature.com/reprints.

https://doi.org/10.1038/s41558-022-01562-8

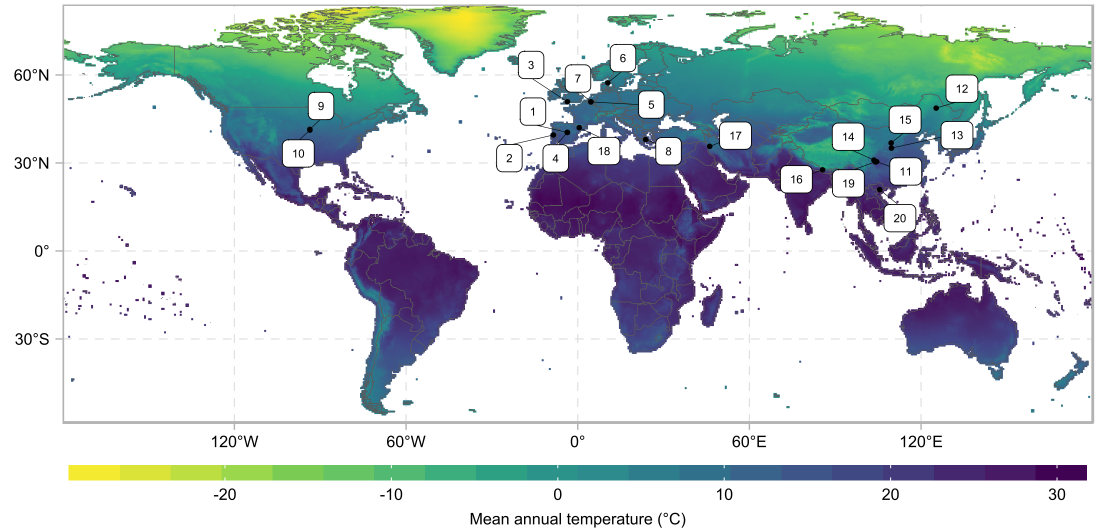

Extended Data Fig. 1 | Locations of the cropland sites in this study. The numbers in squares denote the identification of the catchment. Details of the study sites are provided in Supplementary Table 1.

https://doi.org/10.1038/s41558-022-01562-8

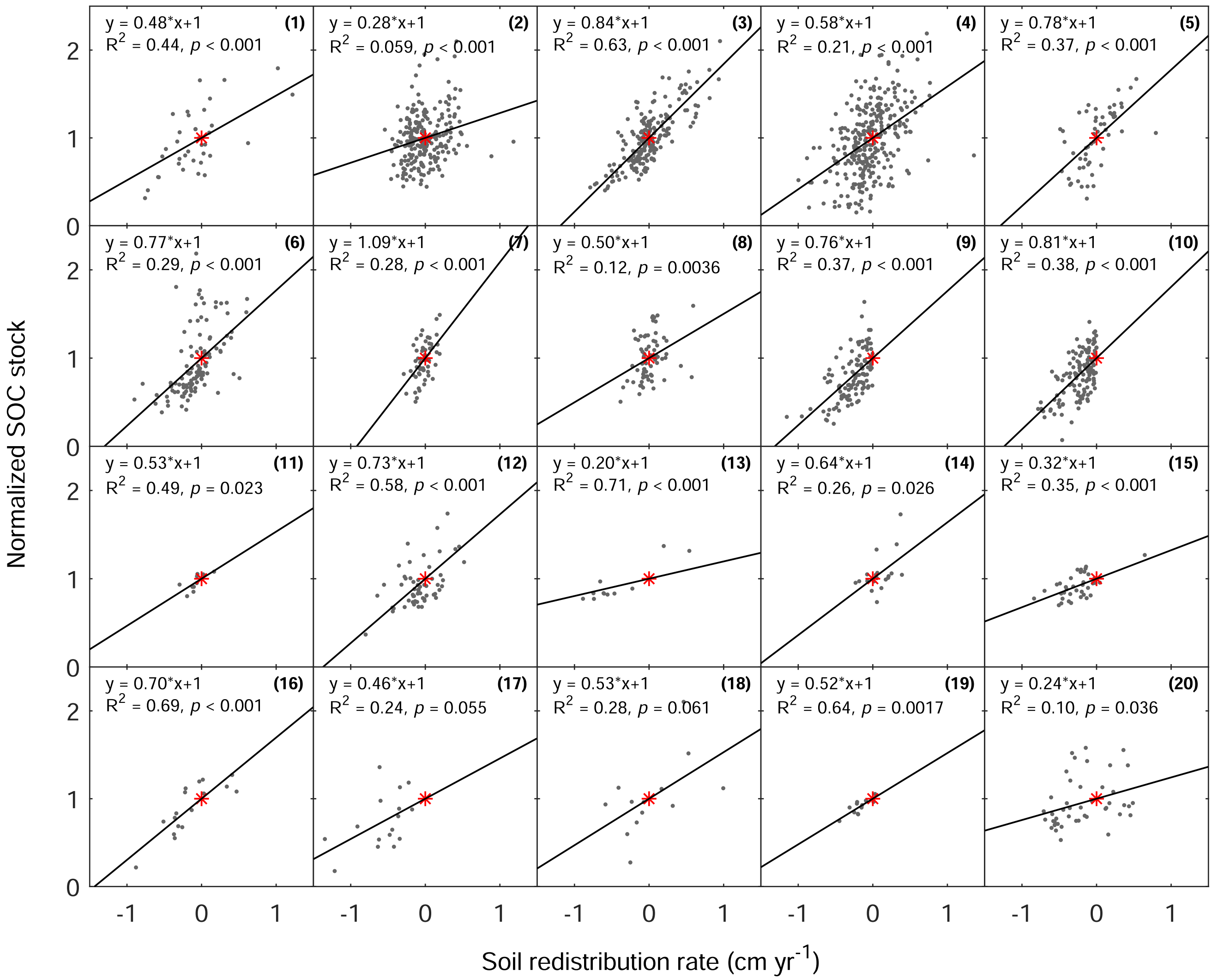

Extended Data Fig. 2 | Relationships between normalized SOC stocks and soil redistribution rates for the cropland sites. Negative values of soil redistribution rates indicate erosion, while the positive values indicate deposition. The SOC stock of each soil profile is normalized by being divided by the SOC stock of the reference sites (as denoted with red asterisks) not subjected to erosion or deposition. The regression lines are set to pass through the reference value so that the sensitivity of normalized SOC stocks to the variation of soil distribution rates can be assessed by comparing the slopes of these linear regression lines. The number in parentheses denote the identification of the catchment, which is shown in Supplementary Table 1.

https://doi.org/10.1038/s41558-022-01562-8

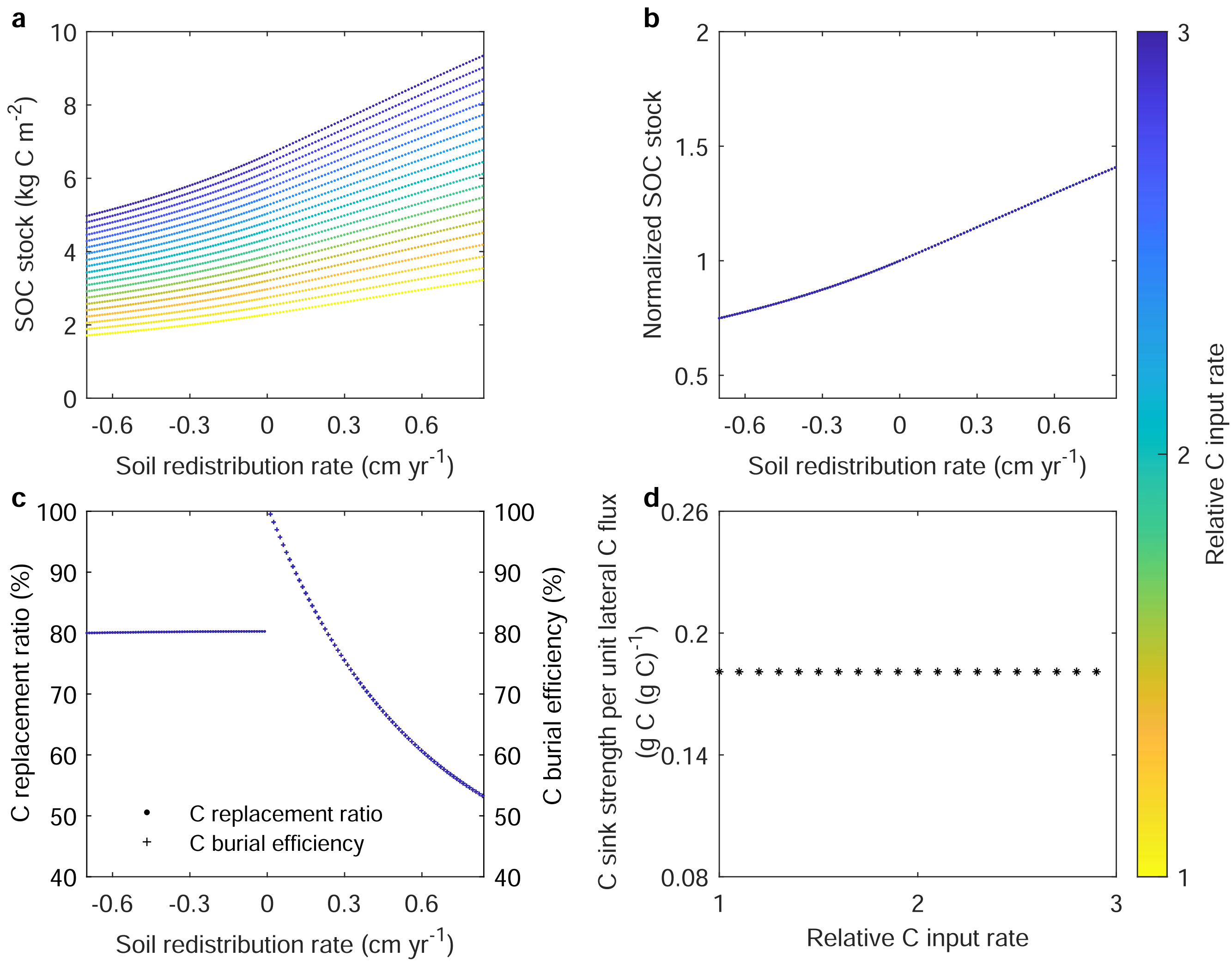

Extended Data Fig. 3 | SOC cycling in eroding croplands in scenarios of various C input rates. a, Variation of SOC stocks with soil redistribution rates. **b**, Variation of the normalized SOC stocks with soil redistribution rates. **c**, Variation of replace ratios of lost SOC due to erosion in the eroding area with soil redistribution rates and variation of burial efficiencies of deposited SOC in the depositional area with soil redistribution rates. **d**, Variation of the erosion-induced C sink per unit lateral C flux with C input rates. In **a**, **b** and **c**, the negative values of soil redistribution rates indicate erosion, while the positive values indicate deposition. In **b**, the SOC stock of each soil profile is normalized by being divided by the SOC stock of the reference sites not subjected to erosion or deposition. For a hillslope with a given soil redistribution pattern, variations in normalized SOC stocks, C replacement and burial efficiency and the C sink strength per unit of lateral SOC flux are independent of the C input rate.

 https://doi.org/10.1038/s41558-022-01562-8

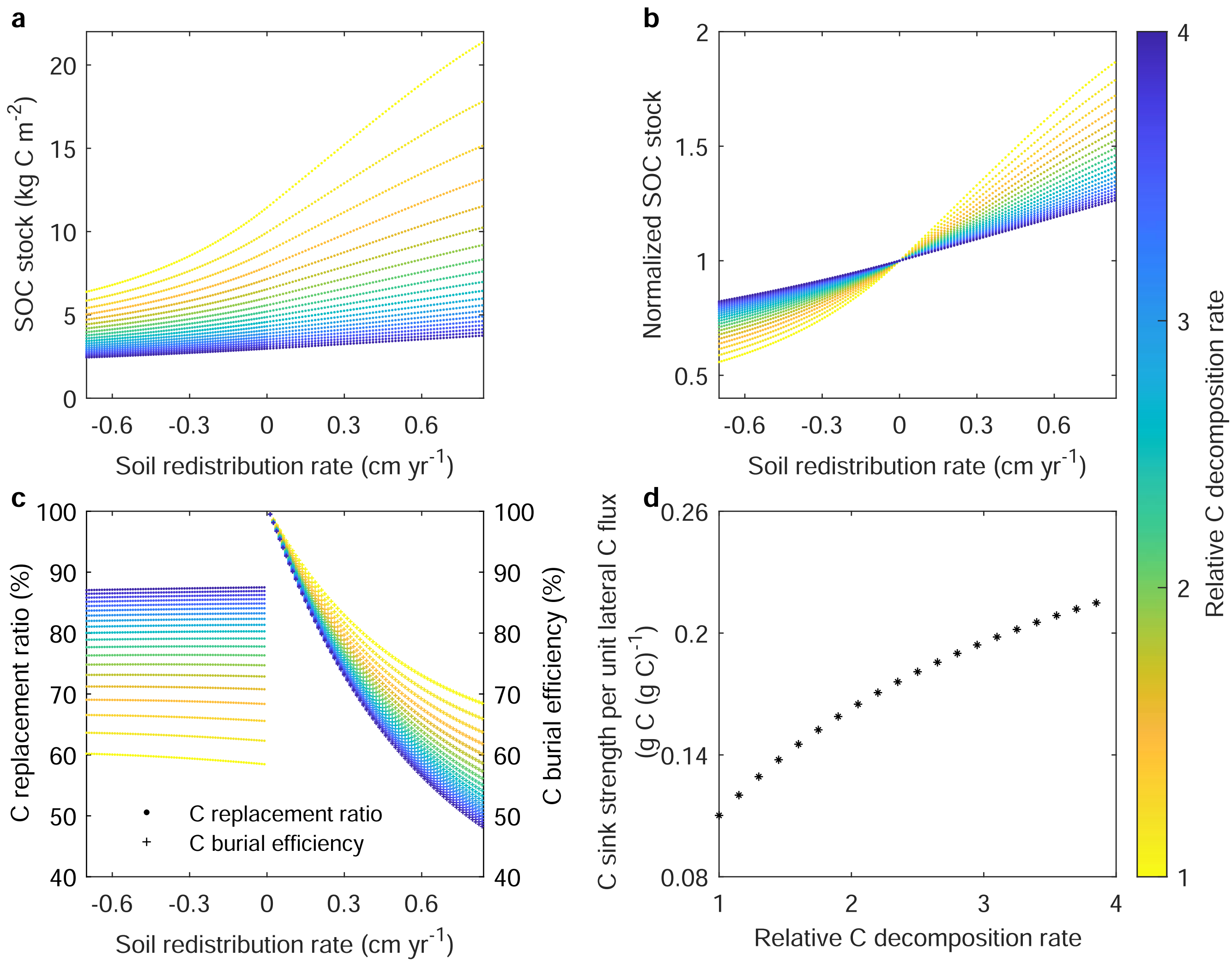

Extended Data Fig. 4 | SOC cycling in eroding croplands in scenarios of various C decomposition rates. a, Variation of SOC stocks with soil redistribution rates. **b**, Variation of the normalized SOC stocks with soil redistribution rates. **c**, Variation of replace ratios of lost SOC due to erosion in the eroding area with soil redistribution rates and variation of burial efficiencies of deposited SOC in the depositional area with soil redistribution rates. **d**, Variation of the erosion-induced total C sink per unit lateral C flux with C decomposition rates. In **a**, **b** and **c**, the negative values of soil redistribution rate indicate erosion, while the positive values indicate deposition. In **b**, the SOC stock of each soil profile is normalized by being divided by the SOC stock of the reference sites not subjected to erosion or deposition.

https://doi.org/10.1038/s41558-022-01562-8

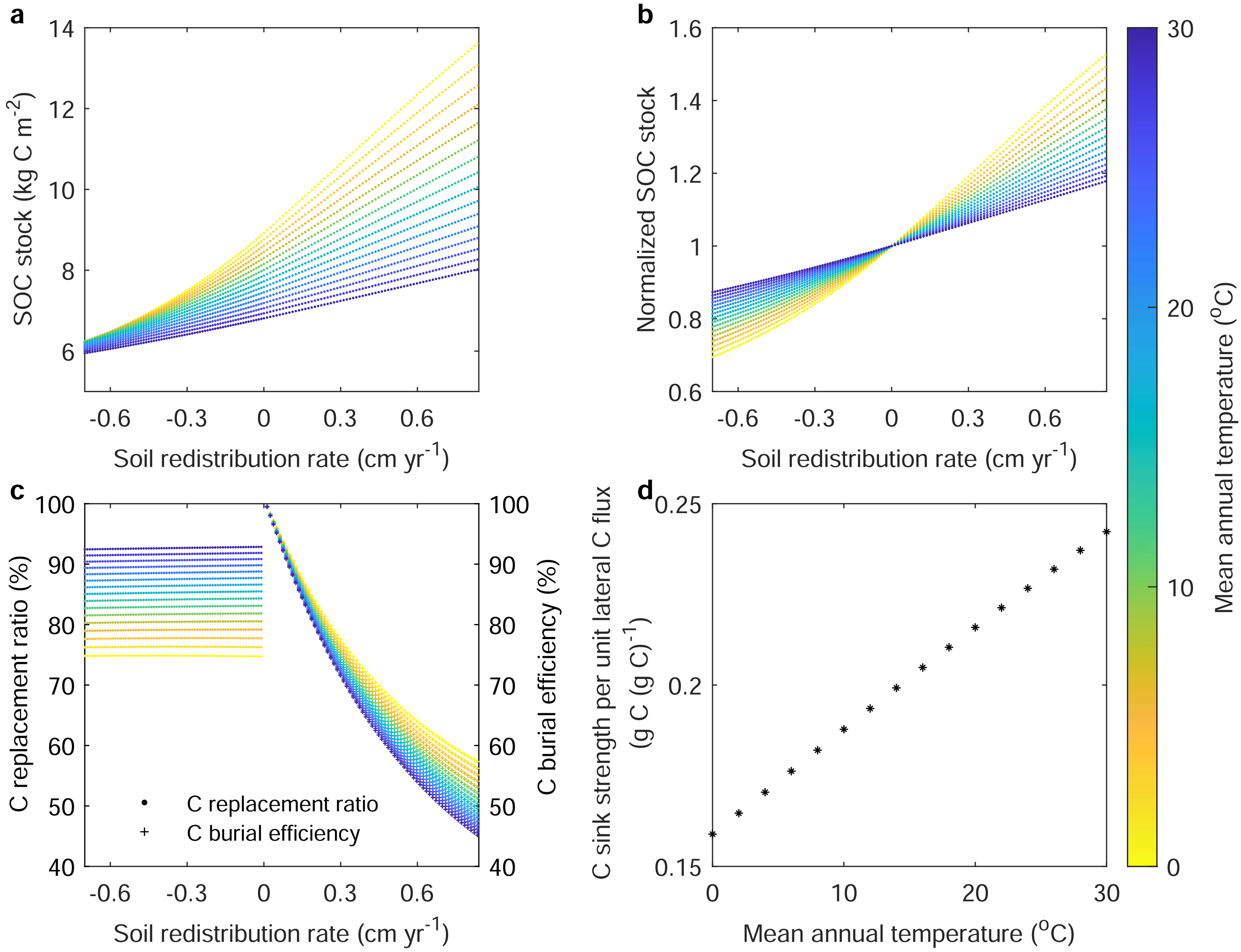

Extended Data Fig. 5 | SOC cycling in eroding croplands in scenarios of varying temperature. a, Variation of SOC stocks with soil redistribution rates. **b**, Variation of the normalized SOC stocks with soil redistribution rates. **c**, Variation of replacement ratio of lost SOC due to erosion in the eroding area with soil redistribution rates and variation of burial efficiency of deposited SOC in the depositional area with soil redistribution rates. **d**, Variation of the erosion-induced C sink per unit lateral C flux with temperature. In **a**, **b** and **c**, the negative values of soil redistribution rate indicate erosion, while the positive values indicate deposition. In **b**, the SOC stock of each soil profile is normalized by being divided by the SOC stock of the reference sites not subjected to erosion or deposition.

https://doi.org/10.1038/s41558-022-01562-8

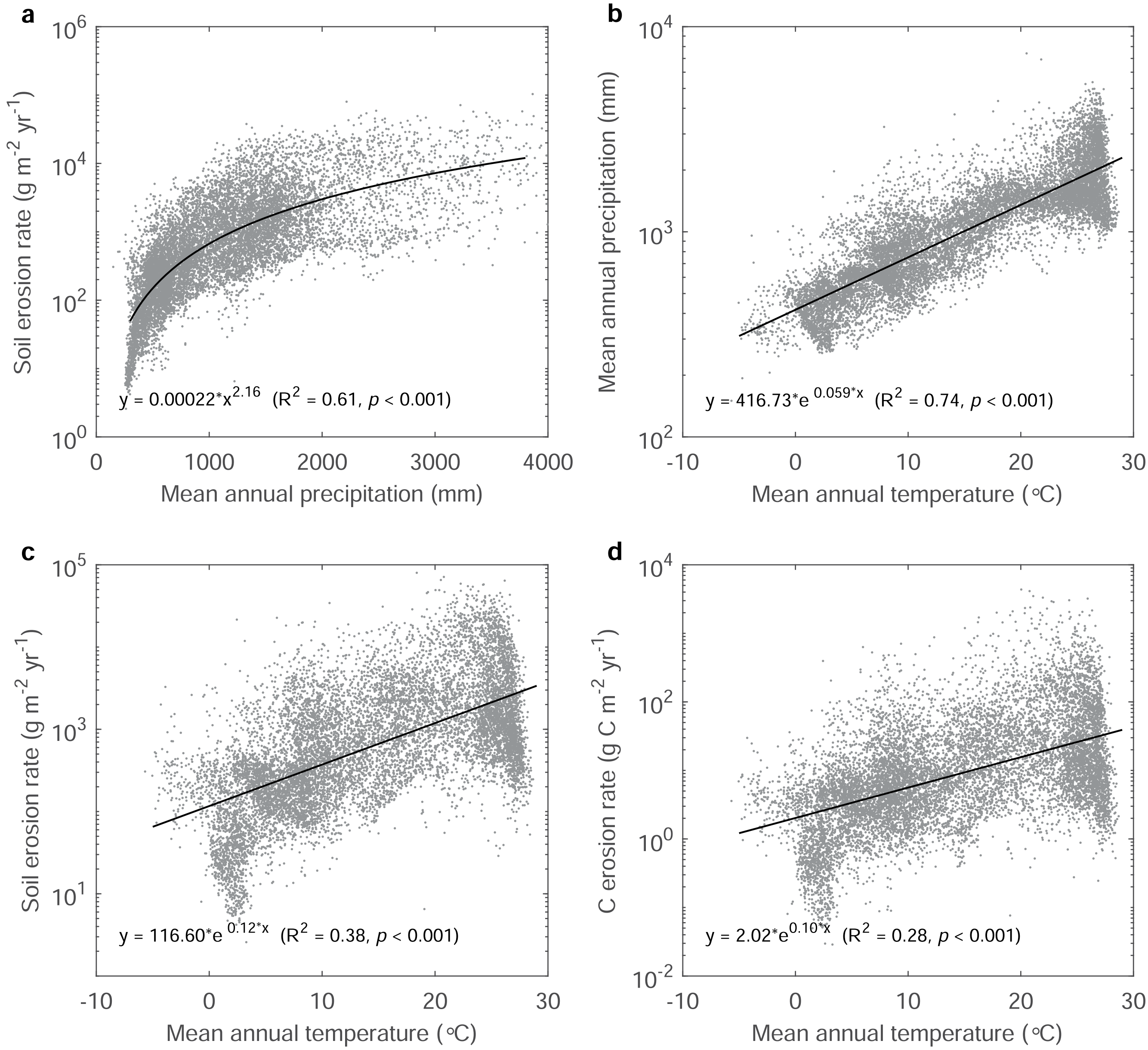

Extended Data Fig. 6 | Relationships between erosion and climatic factors in croplands derived from a global estimation of agricultural erosion[21]. **a**, Soil erosion rate versus mean annual precipitation. **b**, Mean annual precipitation versus mean annual temperature. **c**, Soil erosion rate versus mean annual temperature. **d**, C erosion rate versus mean annual temperature.

https://doi.org/10.1038/s41558-022-01562-8

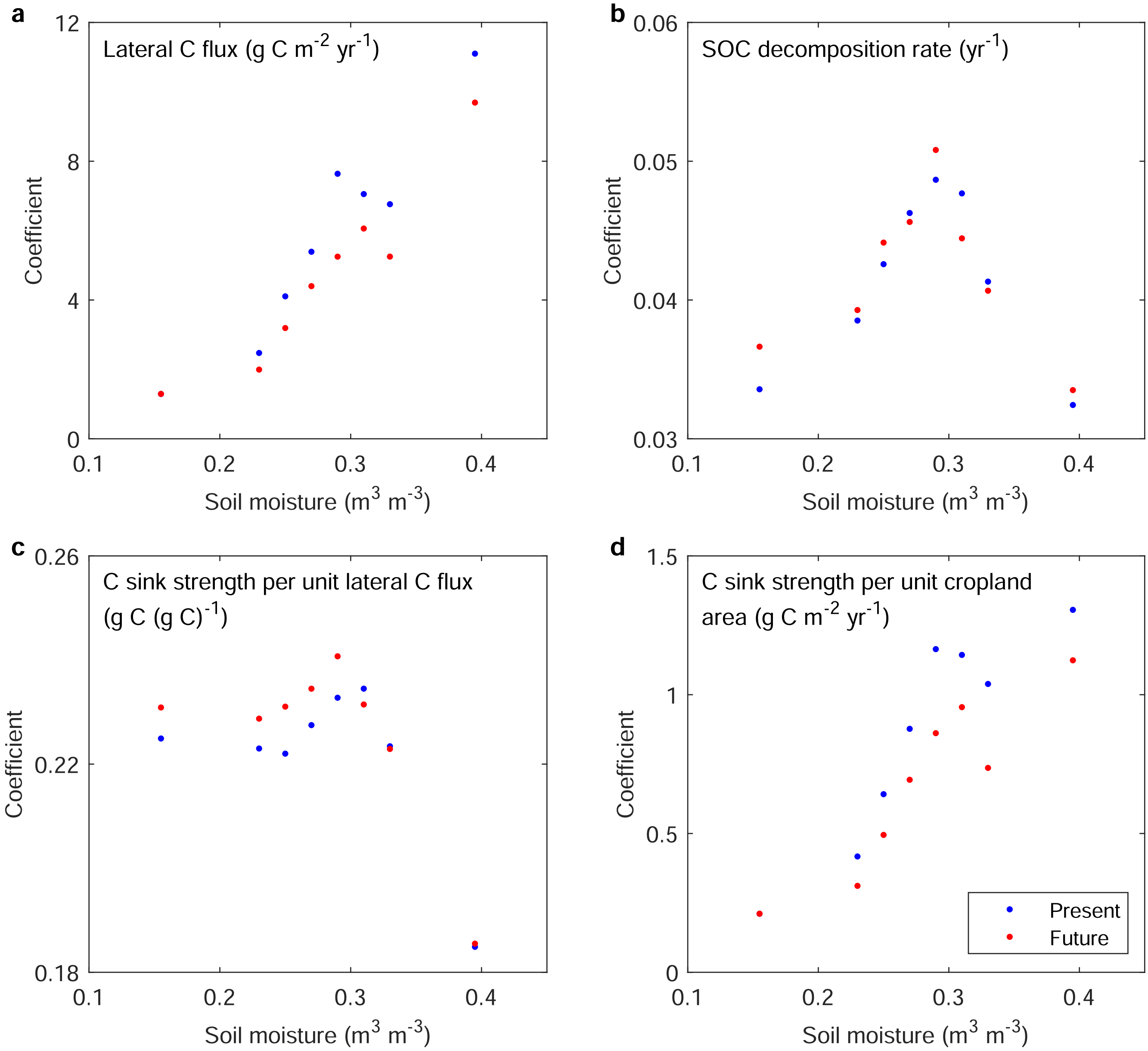

Extended Data Fig. 7 | The effects of soil moisture on the relationships between temperature and various SOC cycling metrics. a, The relationship between soil moisture and the coefficient denoting the sensitivity of lateral SOC fluxes caused by erosion to the variation of mean annual temperature. Details of the regression between lateral SOC fluxes by erosion and temperature under various soil moisture conditions are displayed in Supplementary Fig. 3. **b**, The relationship between soil moisture and the coefficient denoting the sensitivity of SOC decomposition rates to the variation of mean annual temperature. Details of the regression between SOC decomposition rates and temperature under various soil moisture conditions are displayed in Supplementary Fig. 4. **c**, The relationship between soil moisture and the coefficient denoting the sensitivity of the C sink strength per unit lateral SOC flux to the variation of mean annual temperature. Details of the regression between the C sink strength per unit lateral SOC flux and temperature under various soil moisture conditions are displayed in Supplementary Fig. 5. **d**, The relationship between soil moisture and the coefficient denoting the sensitivity of the C sink strength per unit cropland area to the variation of mean annual temperature. Details of the regression between the C sink strength per unit cropland area and temperature under various soil moisture conditions are displayed in Supplementary Fig. 6.